SnSe + Ag_2Se composite engineering with ball milling for enhanced thermoelectric performance

SnSe + Ag_2Se composite engineering with ball milling for enhanced thermoelectric performance

Dan Feng[1,2], Yue-Xing Chen[2, 4], Liang-Wei Fu[2,4], Ju Li[1,3], Jia-Qing He[2,]*(0000-0003-3954-6003)

[1]State Key Laboratory for Mechanical Behavior of Materials and Frontier Institute of Science and Technology, Xi'an Jiaotong University, Xi'an 710049, China.

[2]Shenzhen Key Laboratory of Thermoelectric Materials，Department of physics, South University of Science and Technology of China, Shenzhen 518055, China.

[3]Department of Nuclear Science and Engineering and Department of Materials Science and Engineering, Massachusetts Institute of Technology, Cambridge, Massachusetts 02139, USA

[4]Key Laboratory of Artificial Micro- and Nano-Structures of Ministry of Education and School of Physics and Technology, Wuhan University, Wuhan 430072, China

Email: he.jq@sustc.edu.cn

Abstract Earth-abundant IV-VI semiconductor SnSe is regarded as a promising thermoelectric material due to its intrinsic low thermal conductivity. In this report, the highly textured SnSe/Ag_2Se composites were first designed by solid solution method followed by spark plasma sintering (SPS) and their thermoelectric properties in two directions were investigated, and then the performance of composites was further optimized with an additional ball milling. The co-existence of SnSe and Ag_2Se phases is clearly confirmed by energy dispersive X-ray spectroscopy (EDX) in transmission electron microscopy (TEM). After ball milling, the size of SnSe grains as well as the incorporated Ag_2Se particles reduces effectively, which synergistically optimizes the electrical and thermal transport properties at high temperature range. As a result, a maximum *ZT* of ~ 0.74 at 773 K for SnSe+1%Ag_2Se in the direction vertical to the pressing direction is achieved. Composite engineering with additional ball milling is thus proved to be an efficient way to improve the thermoelectric properties of SnSe, and this strategy could be applicable to other thermoelectric systems.

Keywords Thermoelectrics; SnSe; composite engineering; ball milling

1 Introduction

Thermoelectric (TE) materials, which could directly convert heat into electrical energy and vice versa, are deemed as promising materials for applications in thermoelectric power generators and refrigerators.[1-3] Generally, the TE conversion efficiency is depended on the figure of merit (*ZT*) defined as $ZT=S^2\sigma T/\kappa$, where S, σ, T, κ and $S^2\sigma$ are the Seebeck coefficient, electrical conductivity, absolute temperature, thermal conductivity and power factor, respectively. The most common approaches for pursuing high *ZT* values include maximizing high power factor by band engineering, such as resonant doping,[4] modulation doping,[5] band convergence/degeneracy,[3, 6] etc., or minimizing the thermal conductivity through all-scale hierarchical structuring,[7] nano-structuring,[8] etc. The widely investigated IV-VI semiconductors lead chalcogenides (PbTe, PbSe and PbS) performed the best TE properties at medium temperature range from 573 to 773 K.[9-15] Besides, SnTe compound, which possesses similar crystal structure and valence band characteristics with PbTe and owns narrow band gap (E_g ~ 0.3 eV), also shows potential to be a good thermoelectric material.[16-20] However, the use of Pb and Te elements limits their further development due to the toxicity and high-cost.

Tin selenide (SnSe), another IV-VI compound,

crystalizes with a layered structure with orthorhombic symmetry (*Pnma* space group), and undergoes a phase transition at ~ 800 K to a higher symmetry orthorhombic symmetry (*Cmcm* space group). SnSe could be a topological crystalline insulator at low temperature[21], devices based on this materials have been widely applied, such as photovoltaic applications,[22] memory switching devices,[23] anode materials for lithium batteries,[24] etc. In recent years, SnSe is regarded as a promising thermoelectric material since a record high *ZT* of ~ 2.6 was achieved in its single crystal along *b*-axis at 923 K,[25] and also the highest ZT_{dev} ~ 1.34 was realized in hole-doped single crystalline SnSe from 300 to 773 K.[26] However, the time consuming and poor mechanical properties seriously prevented the practical use of SnSe single crystals. The study on polycrystalline SnSe thus attracted lots of attentions,[27-32] although the TE performance of pristine polycrystalline SnSe is not competitive, which is mainly due to the poor electrical transport properties caused by the intrinsic low carrier concentration of ~ 1×10^{17} cm^{-3}.[33] In order to optimize the carrier concentrations and improve the TE properties of polycrystalline SnSe, trials of doping and alloying were conducted hitherto. For instance, substituting Sn with Ag is proved to be an effective way to introduce p-type carriers, and the *ZT* value of $Ag_{0.01}Sn_{0.99}Se$ is found to be 0.6 at 750 K;[27] Alkali metal such as Na or K has been introduced in SnSe to lift up the hole carrier concentrations, leading to a peak *ZT* ~ 0.8 in $Na_{0.015}Sn_{0.985}Se$ and ~1.1 in $K_{0.01}Sn_{0.99}Se$ at 773 K, respectively.[28, 32] In addition, Na and Te co-doped p-type $Sn_{0.99}Na_{0.01}Se_{0.84}Te_{0.16}$ obtained a maximum *ZT* of 0.72 at 773 K due to the reduced thermal conductivity by alloy scattering of phonons and increased carrier concentration by Na-doping.[34] For S and I co-doped n-type $SnSe_{0.87}S_{0.1}I_{0.03}$ sample, a maximum *ZT* ~ 1.0 at 773 K is obtained benefiting from the lower thermal conductivity and enhanced Seebeck coefficient,[35] etc.

Moreover, composite engineering is also considered as an effective method to optimize TE materials.[36, 37] SnSe composite with SiC particles formed phonon-scattering center, leading to a decreased thermal conductivity, and a maximum *ZT* of 0.125 at 300 K.[38] On the other hand, SnSe composites with 2D $MoSe_2$ improved electrical properties and a *ZT* of 0.5 at 773 K was obtained.[39] Considering the superior performance of Ag doping and huge potential profit of composite engineering in SnSe, in this contribution, we investigated the TE properties of SnSe/Ag_2Se composites. The prepared anisotropic polycrystalline samples were measured in two different directions, and the incorporation of Ag_2Se is proved to be an effective method to enhance the TE properties of SnSe, especially in the direction vertical to the pressing direction. The two samples with a better performance were further optimized by adding a ball milling processing after solid solution, resulting in higher carrier concentration and lower thermal conductivity simultaneously in high temperature range, leading to a maximum *ZT* of ~ 0.74 for SnSe+1 %Ag_2Se at 773 K. This value is higher than any other Ag doped polycrystalline SnSe at the same temperature.[27, 40, 41]

2.1 Experimental

Reagents: Sn powder (99.5%, Aladdin), Se powder (99+%, Alfa Aesar), Ag_2Se powder (Aldrich).

Synthesis: Samples with nominal compositions of SnSe + *x* mol %Ag_2Se (*x* = 0, 0.5, 1.0 and 3.0) were synthesized by the solid solution method with raw materials loaded and sealed into evacuated quartz ampoules (~ 1×10^{-4} Pa), then slowly heated to 950 ℃ in 9.5 h, soaked at this temperature for 24 h and slowly cooled down to room temperature. The ingots were ground into powders by hand milling at first (Samples labeled by HM). Then, SnSe + *x* %Ag_2Se (*x* = 0.5, 1.0) were refined by a planetary ball mill (QM-3SP2, Nanjing University, China) in a nitrogen atmosphere for further optimization (Samples labeled by BM). In the ball milling process, stainless steel vessels and balls were used, and the weight ratio of ball to powder was 20:1. Then the obtained powders were consolidated using spark plasma sintering (SPS-211Lx, Japan) at 723 K for 5 min with a 50 MPa uniaxial pressure.

X-ray Diffraction: The phase structures were investigated by X-ray diffractometer (XRD, Rigaku, Tokyo, Japan) at a scanning rate of 4(°) ·min^{-1}.

Thermoelectric properties: The Seebeck coefficient

and the electrical resistance were simultaneously measured using an Ulvac Riko ZEM-3 instrument under a rare helium atmosphere. The thermal conductivity was calculated by $\kappa = DC_p\rho$, where the thermal diffusivity coefficient (D) was measured using the laser flash diffusivity method in a Netzsch LFA457 (NETZSCH, LFA457, Germany), the density (ρ) was determined by the Archimedes method, and C_p is the specific heat capacity obtained from previous research.[25]

Electron Microscopy: The microstructure was investigated by field emission scanning electron microscope (FESEM, Zeiss Merlin, Germany) with operation voltage of 5 kV, and transmission electron microscope (TEM) investigations were carried out using a FEI Tecnai F30 microscope operated at 300 kV in South University of Science and Technology of China. The thin TEM specimens were prepared by conventional standard methods. The procedures include cutting, grinding, dimpling, polishing and Ar-ion milling on a liquid nitrogen cooling state subsequently.

Hall measurement: The Hall coefficients (R_H) were measured by the van der Pauw method on a commercial Hall Effect measurement system (Lake Shore 8400 Series). Hall carrier concentration (n_H) was then estimated to be equal to $1/eR_H$ and Hall carrier mobility (μ_H) was calculated according to the equation: $\mu_H = R_H\sigma$.

3 Results and discussion

To find the suitable composite amount, SnSe + x %Ag_2Se (x = 0, 0.5, 1.0 and 3.0) were firstly obtained by hand milling (HM) and SPS. Figure 1a, b presents the bulk XRD patterns of SnSe + x %Ag_2Se measured in the planes vertical and parallel to the press direction, respectively. As shown, the main peaks of all the samples are well indexed as the low temperature SnSe phase with orthorhombic structure in *Pnma* space group (PDF No.48-1224). Attributed to the layered structure, the bulk samples are significantly textured, which is clearly reflected in XRD intensity variations and layered collapsing features observed in the moderate-magnification SEM images (Figs. S1 and S2). As shown, compared with standard card information (PDF No.48-1224) of SnSe, the intensities in (4 0 0) plane are exceptionally high in the vertical direction, thus anisotropic features can be expected.

The thermoelectric properties were investigated from 323 to 723 K in both parallel direction (filled symbols) and vertical direction (open symbols), respectively. The schematic diagram of measurement directions is inserted in Fig. 2e. The temperature dependent of electrical conductivity for SnSe + x %Ag_2Se (x = 0-3) samples are plotted in Fig. 2a. Compared with pristine SnSe, the incorporation of Ag_2Se effectively increases the electrical conductivity in both directions. The corresponding carrier concentration and mobility are listed in Table 1. Attributed to the textured features, higher mobility in vertical direction is achieved, and thus all the samples exhibit higher electrical conductivity in this direction. Moreover, in both directions, the electrical conductivities have a similar trend with temperature increasing, that is, slightly increase from 323 to ~ 400 K, then decrease to a minimum value at ~ 600 K, and upturn at high temperature. This trend is well explained in previous reports.[30] As shown, SnSe+0.5%Ag_2Se in vertical direction achieves the highest electrical conductivity from room temperature to 473 K among all the samples, the maximum electrical conductivity of ~ 69.31 $S\cdot cm^{-1}$ is obtained at 373 K.

The temperature dependent of Seebeck coefficient is shown in Fig. 2b. The positive Seebeck coefficient values in the entire temperature range for all the samples, indict p-type semiconductor behaviors (the dominant charge carrier is hole), which are originated from easily produced Sn vacancies. It is noticed that the Seebeck coefficient of composited samples first increases from 323 to ~ 600 K, but slightly decreases in high temperature, which is possibly due to the bipolar effect. The rising temperature promotes minority carrier jumps across the band gap and offsets the majority ones, leading to the increasement in carrier concentration. Moreover, Ag_2Se achieves higher carrier concentration compared with SnSe,[42] thus the Seebeck coefficient of composited samples are basically lower than pristine SnSe.

Attributed to the remarkable enhancement in electrical conductivity and comparable Seebeck coefficient, the composite samples achieve higher power factor in vertical direction than that in parallel direction as shown in Fig.

2c. The tendency of the temperature dependent power factor is similar to the electrical conductivity, and all the composite samples show better performance in moderate temperature (around 423 K). In this system, SnSe+0.5%Ag_2Se exhibits the highest power factor over the entire temperature range, the peak value of ~ 573 $\mu W \cdot m^{-1} \cdot K^{-2}$ is obtained at 423 K.

Figure 2d shows the total thermal conductivity of SnSe + *x* %Ag_2Se (x=0, 0.5, 1.0 and 3.0) in two directions. All the samples exhibit a decreasing trend from 323 to 723 K, and due to the higher mobility, samples measured in vertical direction achieve higher thermal conductivity. As known, the total thermal conductivity (κ_{tot}) consists of electronic thermal conductivity (κ_{ele}) and lattice thermal conductivity (κ_{lat}). The electrical thermal conductivity can be calculated by Wiedemann-Franz law, $\kappa_{ele}=L\sigma T$, where L is the Lorenz number, σ is the electrical conductivity, and T is the operating temperature, then the lattice thermal conductivity is obtained by subtracting electronic thermal conductivity from total thermal conductivity, $\kappa_{lat}=\kappa_{tot}-\kappa_{ele}$. The lattice thermal conductivity is plotted in Fig. 2e. As shown in Fig. 2a, although compositing with Ag_2Se effectively enhances the electrical conductivity, the value is still relatively low, leading to negligible electrical thermal conductivities. Thus, the lattice thermal conductivity is dominant in total thermal conductivity.

Benefiting from the better electrical transport properties, samples in vertical direction exhibit higher *ZT* values as shown in Fig.2f, and SnSe + *x* %Ag_2Se (x = 0.5, 1.0) samples express the highest TE properties in vertical direction. However, the maximum values are only about 0.45 at 723 K. Thus, an additional ball milling process were performed to further optimize the TE properties of SnSe + *x* %Ag_2Se (x = 0.5, 1.0) composites.

To investigate the influence of ball milling applied before SPS on microstructures, it was performed the SEM observation on fresh cleaved surface for SnSe + *x* %Ag_2Se (x = 0.5, 1.0) bulk samples processed by regular hand milling (HM) and ball milling (BM) in two directions. As shown in Fig. 3, the lamellar grains viewed along the vertical direction are clearly characterized. The grains show significant preferred orientations, indicating a strong texture feature, which is consistent with XRD results. As shown in the parallel direction, the grain size of HM samples is tens of microns, as shown in Fig. 3a, e. Ball milling effectively decreases the grain size, which can be easily seen in Fig. 3c, g. In addition, we estimated the texturing degree of HM and BM samples for the (l 0 0) crystal planes by the Lotgering method from XRD results according to following formula (Figs. 1 and S3),[43]

$$F = \frac{(P-P_0)}{(1-P_0)} \quad (1)$$

$$P = \frac{I(l00)}{\sum I(hkl)} \quad (2)$$

$$P_0 = \frac{I_0(l00)}{\sum I_0(hkl)} \quad (3)$$

where P is the ratio of the (l 0 0) intensity and the overall intensity of the measured samples, P_0 is the ratio of the (l 0 0) intensity and the overall intensity of the JCPDS card. As a result, the texturing degree of SnSe+0.5%Ag_2Se-HM and SnSe+1.0%Ag_2Se-HM samples are 0.64 and 0.71, respectively. While the corresponding BM samples are only 0.36 and 0.25. Thus, the reduction in grain size for BM samples doubtlessly lowers the degree of texturing and leads to the lower mobility in the vertical direction which will be discussed in the following TE properties analysis.

As discussed in Fig. 2, samples in this system obtained better performance in vertical direction, thus the TE properties of SnSe + *x* %Ag_2Se (x = 0.5, 1) grounded by HM and BM were measured in vertical direction. The TE properties of pristine SnSe in vertical direction are also plotted in Fig. 4 as a reference. As shown in Fig. 4a, the BM samples exhibit much lower electrical conductivity from 323 to ~ 600 K compared with HM samples, which is mainly attributed to the lower mobility as plotted in Fig. 5b. But from ~ 600 to 773 K, BM samples achieve higher electrical conductivities, which are caused by the increased carrier concentration in high temperature shown in Fig. 5a. The details will be discussed later. Moreover, BM samples exhibit higher Seebeck coefficient from 323 to ~ 600 K mainly due to the lower carrier concentration

at lower temperature, while HM sample and BM sample obtain similar Seebeck coefficient at high temperature. Thus, the calculated power factor shown in Fig. 4c reveals that ball milling effectively enhances the power factor at high temperature.

Then, the total thermal conductivity and calculated lattice thermal conductivity are shown in Fig. 4d, e, respectively. Owing to the relatively low electrical conductivity, the lattice thermal conductivity dominates the total thermal conductivity. It is known that some of the second phases could be dissolved in the matrix as dopant at high temperature,[36] which leads to higher carrier concentration and creates more point defects. In our system, ball milling reduces the grain size of matrix SnSe as well as composited Ag_2Se, as shown Fig. 6, leading to more boundary defects, thus BM samples obtain higher doping amount and denser point defects at high temperature. As a consequence, the lattice thermal conductivity of BM samples shows obvious reduction at high temperatures as illustrated in Fig. 4e, which is favorable to TE properties.

As a result, BM samples achieve higher power factor and lower thermal conductivity at the same time at high temperature (673 - 773 K) than HM samples, leading to much higher *ZT* value as plotted in Fig. 4f. Especially, *ZT* value of SnSe+1%Ag_2Se sample reaches a maximum of ~ 0.74 at 773 K, which is much higher than 0.45 for pristine SnSe at same temperature, and 23% higher than Ag-doped SnSe (~0.6 at 750 K) in previous report.[27]

To better understand the transport properties of SnSe + *x* %Ag_2Se (*x* = 0.5, 1.0) grounded by HM and BM, the carrier concentration and mobility of these four samples were measured in the vertical direction using the van der Pauw method. As shown in Fig. 5a, the carrier concentration of both HM and BM samples are significantly enhanced at high temperature, possibly because some of the composited Ag_2Se dissolve in the SnSe matrix at high temperature, which effectively increases the carrier concentration. Compared with hand milling, ball milling creates more boundaries and facilitates Ag_2Se dissolving into the matrix, as shown in Fig. 6. Thus, BM samples achieve higher carrier concentration at high temperature. In addition, ball milling effectively decreases the grain size as shown in SEM images in Fig. 3, leading to denser boundaries and lower texture degree, thus BM samples shows lower mobility in the vertical direction from 323 to ~ 600 K.

To further confirm the microstructure of Ag_2Se in SnSe matrix, SnSe+1%Ag_2Se grounded by BM was investigated by TEM view along vertical direction. The low-magnification TEM image shows in Fig. 7a clearly reveals the lamellar structure of grains, which is consistent with SEM observations and the anisotropic transport properties. Figure 7b is high-resolution TEM image viewed along [1 0 1] zone axis with corresponding fast Fourier transformation (FFT) pattern (inset). Moreover, X-ray energy dispersive spectroscopy (EDS) in STEM mode was employed to confirm the co-existence of SnSe and incorporated Ag_2Se, as shown in Fig. 7c-g. Figure 7c is high-angle annular-dark-field (HAADF)-STEM micrograph. As known, HAADF image exhibits a $Z^{1.7}$-dependence with respect to the atomic number (*Z*).[44] Thus, the area in the marked box with brighter contrast was chosen to analyze the EDS spectrum. Figure 7d-g provides clear evidence that Ag_2Se and SnSe phases are co-existing in SnSe+1%Ag_2Se sample, where the color blue, orange and green represent Sn, Se and Ag element, respectively. Thus, Ag_2Se is indeed successfully composited in SnSe matrix.

4 Conclusion

In summary, SnSe/*x* %Ag_2Se (*x* = 0, 0.5, 1.0 and 3.0) composites with highly textured features were first prepared by solid solution and SPS to investigate their thermoelectric properties from 323 to 723 K. SnSe + *x* %Ag_2Se (*x* = 0.5, 1) expressed better TE performance were further optimized with an additional ball milling proceeded after solid solution. As a result, the grain size significantly decreases, and the electrical conductivity and thermal conductivity are optimized simultaneously in the high temperature range, leading to a maximum *ZT* of ~ 0.74 at 773 K for SnSe+1%Ag_2Se in the vertical direction. This value is much higher than that of HM sample of ~ 0.45 for pristine SnSe and 23% higher than that of Ag-doped SnSe (0.6 for $Ag_{0.01}Sn_{0.99}Se$ at 750 K).[27] Thus compositing Ag_2Se coupled with ball milling is deemed as an effective method to improve

thermoelectric performance of SnSe, and this approach could be applicable to other thermoelectric systems for further optimization.

Acknowledgements

This work was financially supported by the National Science Foundation(No.DMR-1410636), the Natural Science Foundation of Guangdong Province (No. 2015A030308001), the Leading Talents of Guangdong Province Program (No. 00201517), and the Science, Technology and Innovation Commission of Shenzhen Municipality (Nos. JCYJ20150831142508365, KQTD2016022619565991 and KQCX2015033110182370), the National Natural Science Foundation of China (No. 51632005). This work was also supported by Project funded by China Postdoctoral Science Foundation.

References

[1]Sootsman JR, Chung DY, Kanatzidis MG. New and Old Concepts in Thermoelectric Materials. Angewandte Chemie. 2009;48 (46): 8616.

[2]Snyder GJ, Toberer ES. Complex thermoelectric materials. Nature Materials. 2008; 7(2):105.

[3]Qin P, Qian X, Ge ZH, Zheng L, Feng J, Zhao LD. Improvements of thermoelectric properties for p-type $Cu_{1.8}S$ bulk materials via optimizing the mechanical alloying process. Inorganic Chemistry Frontiers. 2017; 4(7): 1192.

[4]Heremans JP, Jovovic V, Toberer ES, Saramat A, Kurosaki K, Charoenphakdee A, Yamanaka S, Snyder GJ. Enhancement of thermoelectric efficiency in PbTe by distortion of the electronic density of states. Science. 2008; 321(5888):554.

[5]Pei YL, Wu H, Wu D, Zheng F, He J. High Thermoelectric Performance Realized in a BiCuSeO System by Improving Carrier Mobility through 3D Modulation Doping. Journal of the American Chemical Society. 2014; 136(39):13902.

[6]Pei Y, Shi X, Lalonde A, Wang H, Chen L, Snyder GJ. Convergence of electronic bands for high performance bulk thermoelectrics. Nature. 2011; 473(7345):66.

[7]Biswas K, He J, Blum ID, Wu CI, Hogan TP, Seidman DN, Dravid VP, Kanatzidis MG. High-performance bulk thermoelectrics with all-scale hierarchical architectures. Nature. 2012; 489(7416):414.

[8]Vineis CJ, Shakouri A, Majumdar A, Kanatzidis MG. Nanostructured thermoelectrics: big efficiency gains from small features. Advanced materials. 2010; 22(36):3970.

[9]He J, Androulakis J, Kanatzidis MG, Dravid VP. Seeing Is Believing: Weak Phonon Scattering from Nanostructures in Alkali Metal-Doped Lead Telluride. Nano Letters. 2012; 12(1):343.

[10]Wu HJ, Zhao LD, Zheng FS, Wu D, Pei YL, Tong X, Kanatzidis MG, He JQ. Broad temperature plateau for thermoelectric figure of merit ZT>2 in phase-separated $PbTe_{0.7}S_{0.3}$. Nature Communications. 2014; 5:4515.

[11]Wu H, Carrete J, Zhang Z, Qu Y, Shen X, Wang Z, Zhao LD, He J. Strong enhancement of phonon scattering through nanoscale grains in lead sulfide thermoelectrics. NPG Asia Materials. 2014; 6(6):e108.

[12]Girard SN, He J, Zhou X, Shoemaker D, Jaworski CM, Uher C, Dravid VP, Heremans JP, Kanatzidis MG. High performance Na-doped PbTe-PbS thermoelectric materials: electronic density of states modification and shape-controlled nanostructures. Journal of the American Chemical Society. 2011; 133(41):16588.

[13]He J, Zhao LD, Zheng JC, Doak JW, Wu H,. Wang HQ, Lee Y, Wolverton C, Kanatzidis MG, Dravid VP. Role of sodium doping in lead chalcogenide thermoelectrics. Journal of the American Chemical Society. 2013; 135(12):4624.

[14]Korkosz RJ, Chasapis TC, Lo SH, Doak JW, Kim YJ, Wu CI, Hatzikraniotis E, Hogan TP, Seidman DN, Wolverton C, Dravid VP, Kanatzidis MG. High ZT in p-type $(PbTe)_{1-2x}(PbSe)_x(PbS)_x$ thermoelectric materials. Journal of the American Chemical Society. 2014; 136(8):3225.

[15]Zhang Q, Cao F, Liu W, Lukas K, Yu B, Chen S, Opeil C, Broido D, Chen G, Ren Z. Heavy doping and band engineering by potassium to improve the thermoelectric figure of merit in p-type PbTe, PbSe, and $PbTe_{(1-y)}Se_{(y)}$. Journal of the American Chemical Society. 2012; 134(24):10031.

[16]Tan G, Shi F, Hao S, Chi H, Bailey TP, Zhao LD, Uher C, Wolverton C, Dravid VP, Kanatzidis MG. Valence Band Modification and High Thermoelectric Performance in SnTe Heavily Alloyed with MnTe. Journal of the American Chemical Society. 2015; 137(35):11507.

[17]Tan G, Zhao LD, Shi F, Doak JW, Lo SH, Sun H, Wolverton C, Dravid VP, Uher C, Kanatzidis MG. High thermoelectric performance of p-type SnTe via a synergistic band engineering and nanostructuring approach. Journal of the American Chemical Society. 2014; 136(19):7006.

[18]Tan G, Shi F, Sun H, Zhao LD, Uher C, Dravid VP, Kanatzidis MG. SnTe-$AgBiTe_2$ as an efficient thermoelectric material with low thermal conductivity. Journal of Materials Chemistry A. 2014;

2(48):20849.

[19]Chen Y, Nielsen MD, Gao YB, Zhu TJ, Zhao X, Heremans JP. SnTe–$AgSbTe_2$ Thermoelectric Alloys. Advanced Energy Materials. 2012; 2(1):58.

[20]Zhang Q, Liao B, Lan Y, Lukas K, Liu W, Esfarjani K, Opeil C, Broido D, Chen G, Ren Z. High thermoelectric performance by resonant dopant indium in nanostructured SnTe. Proceedings of the National Academy of Sciences of the United States of America. 2013; 110(33):13261.

[21]Qian XF, Fu L, Li J. Topological Crystalline Insulator Nanomembrane with Strain-Tunable Band Gap. Nano Research. 2015; 8(3): 967.

[22]Antunez PD, Buckley JJ, Brutchey RL. Tin and germanium monochalcogenide IV-VI semiconductor nanocrystals for use in solar cells. Nanoscale. 2011; 3(6):2399.

[23]Chun D, Walser RM, Bené RW, Courtney TH. Polarity-dependent memory switching in devices with SnSe and $SnSe_2$ crystals. Applied Physics Letters. 1974; 24(10):479.

[24]Xue MZ, Yao J, Cheng SC, Fu ZW. Lithium Electrochemistry of a Novel SnSe Thin-Film Anode. Journal of the Electrochemical Society. 2006; 153(2):A270.

[25]Zhao LD, Lo SH, Zhang Y, Sun H, Tan G, Uher C, Wolverton C, Dravid VP, Kanatzidis MG. Ultralow thermal conductivity and high thermoelectric figure of merit in SnSe crystals. Nature. 2014; 508(7496):373.

[26]Zhao LD, Tan G, Hao S, He J, Pei Y, Chi H, Wang H, Gong S, Xu H, Dravid VP. Ultrahigh power factor and thermoelectric performance in hole-doped single-crystal SnSe. Science. 2016; 351(6269):141.

[27]Chen CL, Wang H, Chen YY, Day T, Snyder GJ. Thermoelectric properties of p-type polycrystalline SnSe doped with Ag. Journal of Materials Chemistry A. 2014; 2(29):11171.

[28]Chere EK, Zhang Q, Dahal K, Cao F, Mao J, Ren Z. Studies on Thermoelectric Figure of Merit of Na-doped p-type Polycrystalline SnSe. Journal of Materials Chemistry A. 2016; 4(5):1848.

[29]Ge ZH, Song DS, Chong XY, Zheng FS, Jin L, Qian X, Zheng L, Dunin-Borkowski RE, Qin P, Feng J, Zhao LD. Boosting the thermoelectric performance of (Na, K) co-doped polycrystalline SnSe by synergistic tailoring of the band structure and atomic-scale defect phonon scattering. Journal of the American Chemical Society. 2017; 139(28):9714.

[30]Li Y, Li F, Dong J, Ge Z, Kang F, He J, Du H, Li B, Li JF. Enhanced mid-temperature thermoelectric performance of textured SnSe polycrystals made of solvothermally synthesized powders. Journal of Materials Chemistry C. 2016; 4(10):2047.

[31]Feng D, Ge ZH, Wu D, Chen YX, Wu T, Li J, He J. Enhanced thermoelectric properties of SnSe polycrystals via texture control. Physical Chemistry Chemical Physics. 2016; 18(46):31821.

[32]Chen YX, Ge ZH, Yin M, Feng D, Huang XQ, Zhao W, He J. Understanding of the Extremely Low Thermal Conductivity in High-Performance Polycrystalline SnSe through Potassium Doping. Advanced Functional Materials. 2016; 26(37):6836.

[33]Sassi S, Candolfi C, Vaney JB, Ohorodniichuk V, Masschelein P, Dauscher A, Lenoir B. Assessment of the thermoelectric performance of polycrystalline p-type SnSe. Applied Physics Letters. 2014; 104(21):105.

[34]Wei TR, Wu CF, Zhang X, Tan Q, Sun L, Pan Y, Li JF. Thermoelectric transport properties of pristine and Na-doped $SnSe_{1-x}Te_x$ polycrystals. Physical Chemistry Chemical Physics : PCCP. 2015; 17(44):30102.

[35]Zhang Q, Chere EK, Sun J, Cao F, Dahal K, Chen S, Chen G, Ren Z. Studies on Thermoelectric Properties of n-type Polycrystalline $SnSe_{1-x}S_x$ by Iodine Doping. Advanced Energy Materials. 2015; 5(12): 1500360.

[36]Luo Y, Jiang Q, Yang J, Li W, Zhang D, Zhou Z, Cheng Y, Ren Y, He X, Li X. Simultaneous regulation of electrical and thermal transport properties in $CuInTe_2$ by directly incorporating excess ZnX (X = S, Se). Nano Energy. 2016; 32:80.

[37]Xing ZB, Li JF. Lead-free $AgSn_4SbTe_6$, nanocomposites with enhanced thermoelectric properties by SiC nanodispersion. Journal of Alloys and Compounds. 2016, 687:246.

[38]Ju H, Kim J. Effect of SiC ceramics on thermoelectric properties of SiC/SnSe composites for solid-state thermoelectric applications. Ceramics International. 2016; 42(8):9550.

[39]Huang XQ, Chen YX, Yin M, Feng D, He J. Origin of the enhancement in transport properties on polycrystalline SnSe with compositing two-dimensional material $MoSe_2$. Nanotechnology. 2017; 28(10):105708.

[40]Leng H, Zhou M, Zhao J, Han Y, Li L. Optimization of Thermoelectric Performance of Anisotropic $Ag_xSn_{1-x}Se$ Compounds. Journal of Electronic Materials. 2016; 45(1):527.

[41]Lin CC, Lydia R, Yun JH, Lee HS, Rhyee JS. Extremely low lattice thermal conductivity and point defect scattering of phonons in Ag-doped $(SnSe)_{1-x}(SnS)_x$ compounds. Chemistry of Materials. 2017; 29:5344

[42]Wiegers GA. Electronic and ionic conduction of solid solutions $Ag_{2-x}Au_xSe$ ($0 \le x \le 0.5$). Journal of the Less-Common Metals. 1976; 48(2):269.

[43]Ge ZH, Zhang BP, Shang PP, Li JF. Control of anisotropic electrical transport property of Bi_2S_3 thermoelectric polycrystals. Journal of Materials Chemistry. 2011; 21(25):9194.

[44]Gu L, Zhu C, Li H, Yu Y, Li C, Tsukimoto S, Maier J, Ikuhara Y. Direct Observation of Lithium Staging in Partially Delithiated $LiFePO_4$ at Atomic Resolution. Journal of the American Chemical Society. 2011; 133(13):4661.

TOC

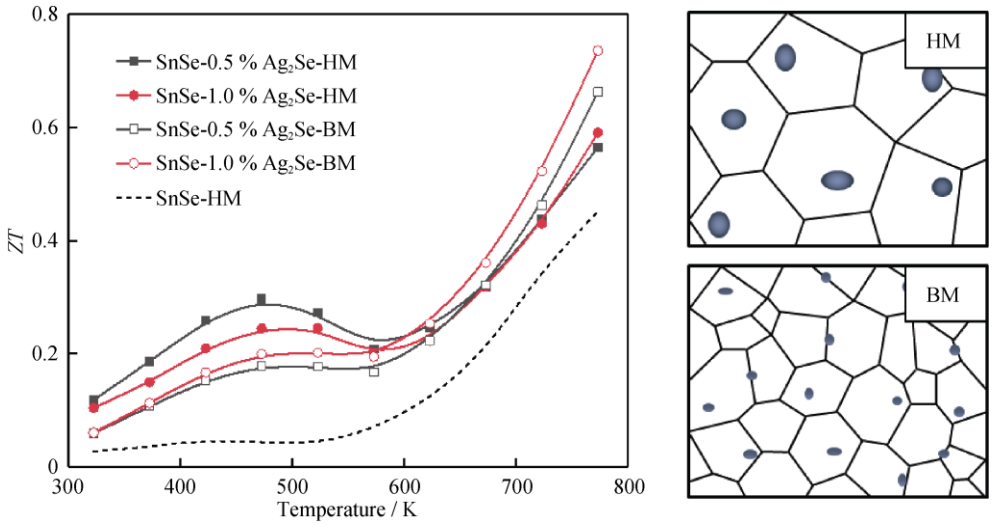

Figures

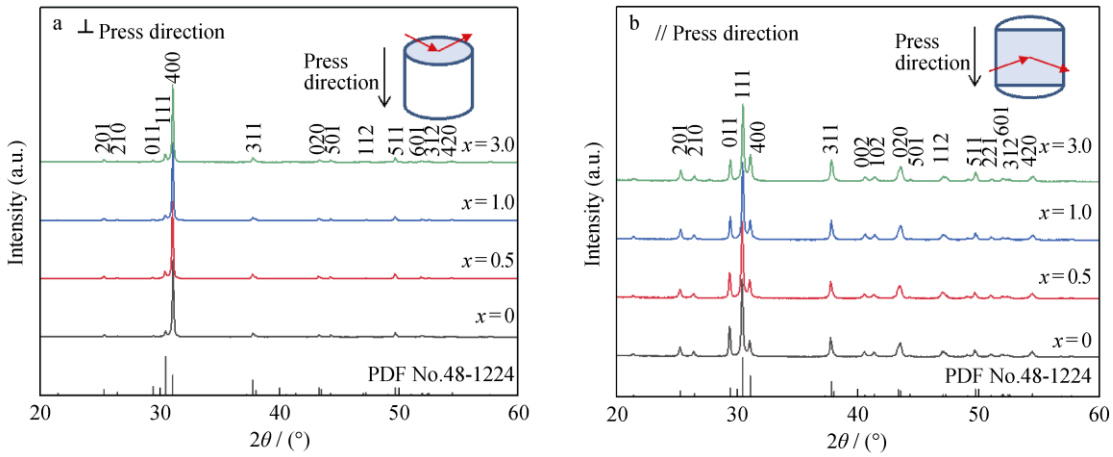

Fig.1 XRD patterns showing SnSe + *x* %Ag_2Se (*x*=0, 0.5, 1.0 and 3.0) crystalize into a *Pnma* (PDF No.48-1224) structure.

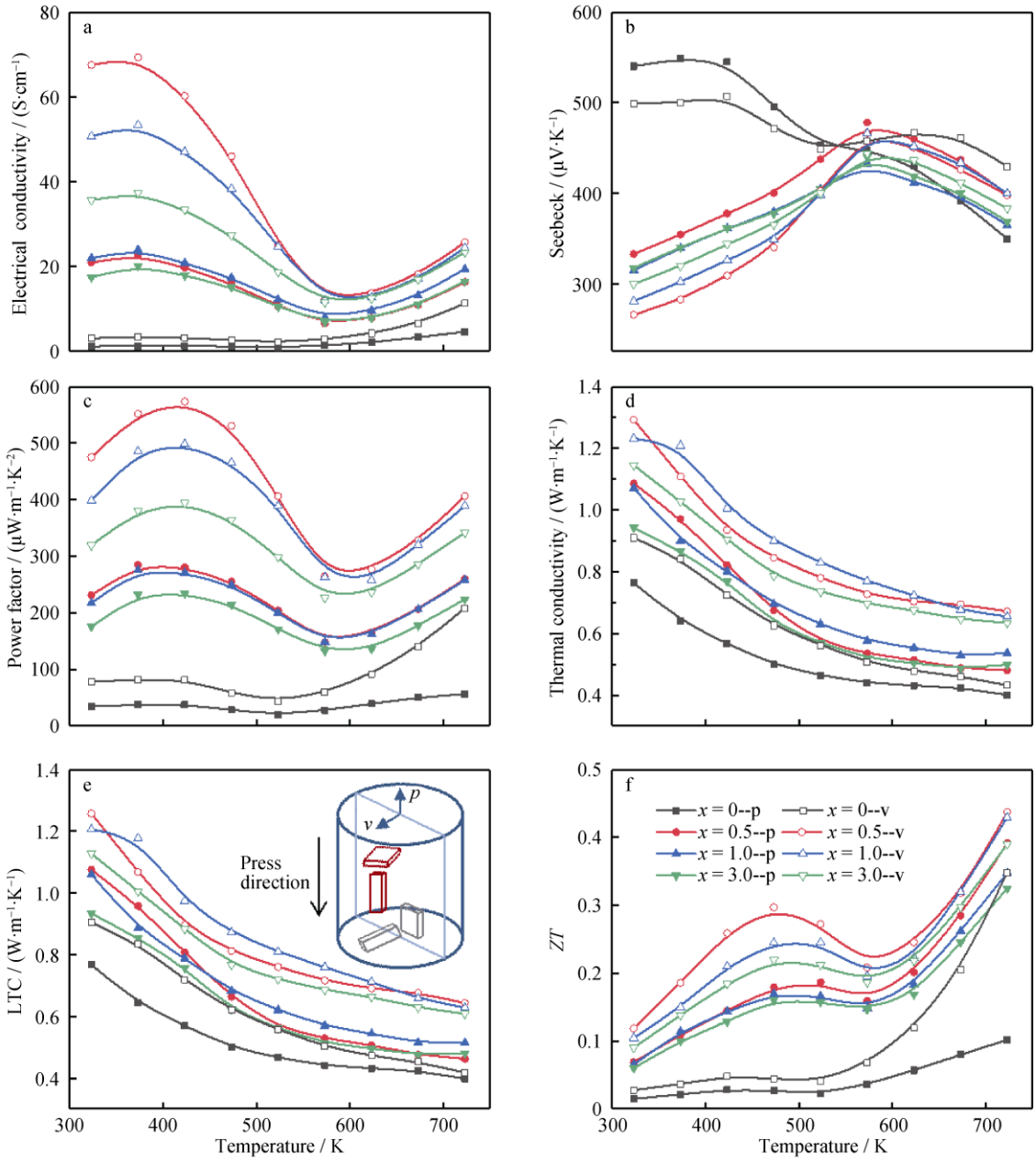

Fig.2 Thermoelectric properties of SnSe + *x* %Ag_2Se (*x*=0, 0.5, 1.0 and 3.0) measured parallel (filled symbols) and vertical (open symbols) to press direction: **a** electrical conductivity, **b** Seebeck coefficient, **c** power factor, **d** total thermal conductivity, **e** lattice thermal conductivity (LTC), and **f** figure of merit *ZT*

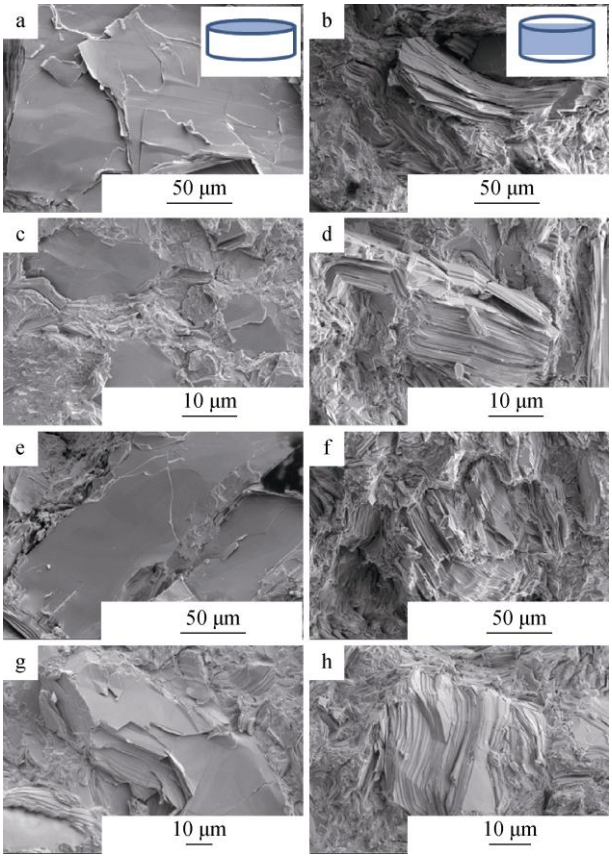

Fig.3 SEM images of SnSe + *x* %Ag_2Se (*x*=0.5, 1) conducted by hand milling and ball milling viewed along parallel direction and vertical direction: **a, b** SnSe + 0.5 %Ag_2Se-HM, **c, d** SnSe + 0.5 %Ag_2Se-BM, **e, f** SnSe + 1.0 %Ag_2Se-HM, and **g, h** SnSe + 1.0 %Ag_2Se-BM

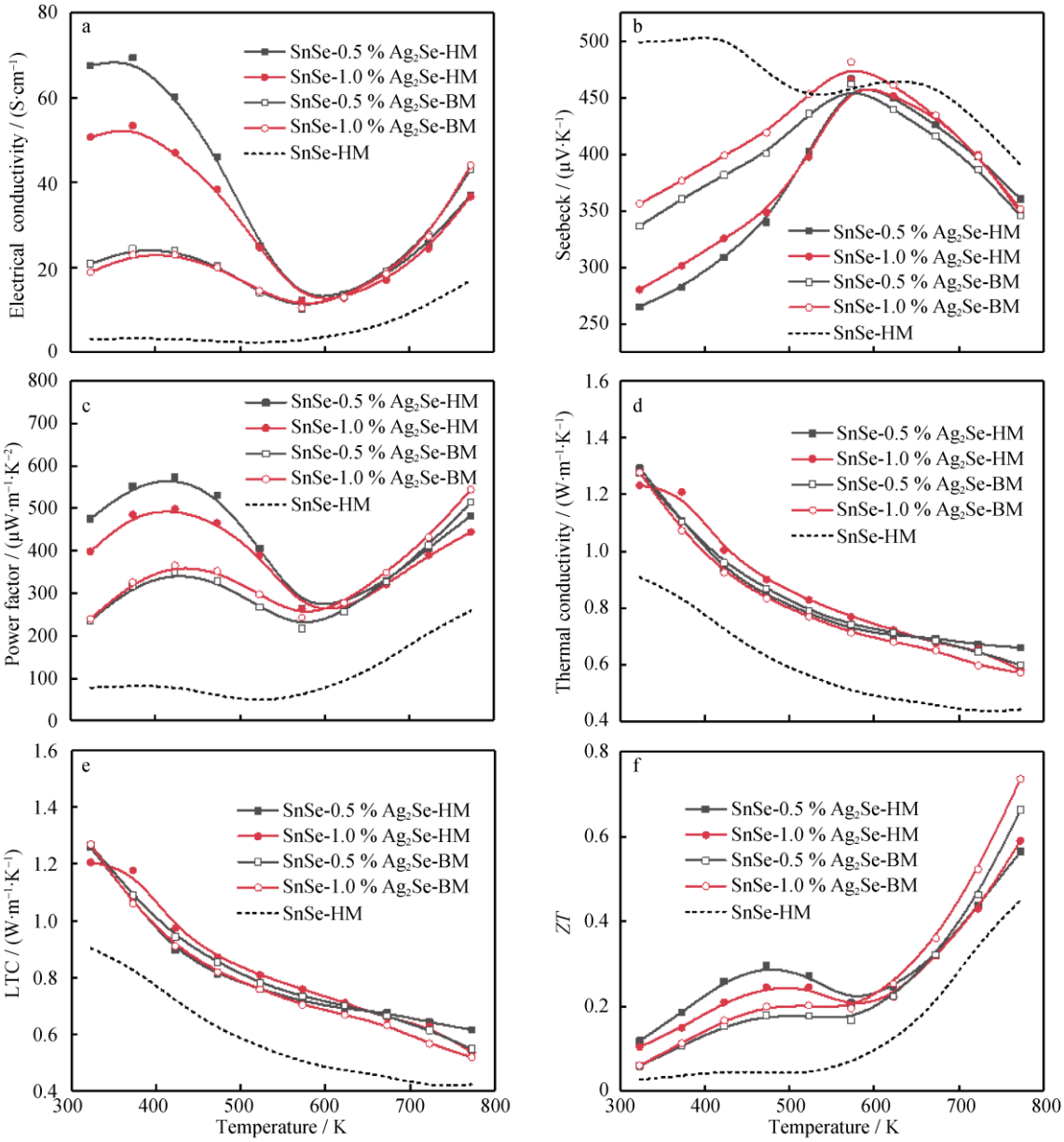

Fig.4 Thermoelectric properties of SnSe + *x* %Ag_2Se (*x*=0.5, 1) conducted by hand milling (filled symbols) and ball milling (open symbols) measured vertical to press direction: **a** electrical conductivity, **b** Seebeck coefficient, **c** power factor, **d** total thermal conductivity, **e** lattice thermal conductivity (LTC), and **f** figure of merit *ZT*

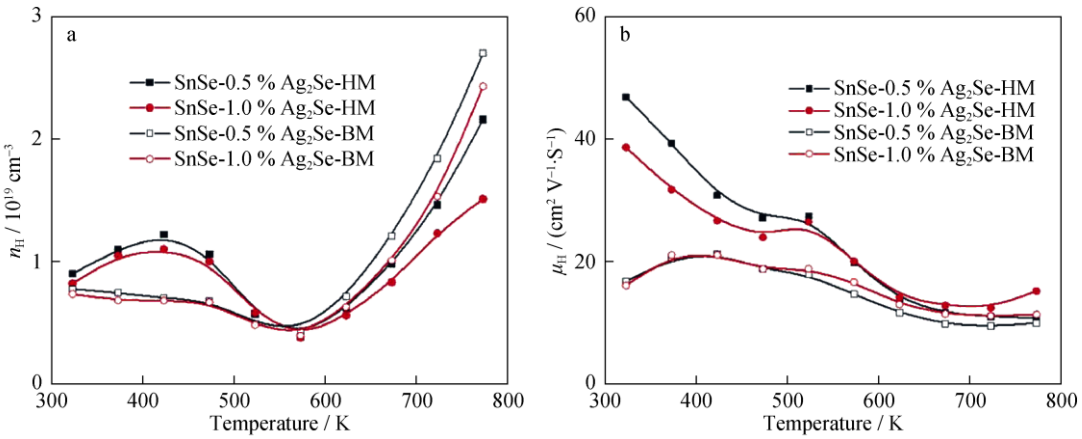

Fig.5 **a** Carrier concentration and **b** mobility of SnSe + *x* %Ag_2Se (*x*=0.5, 1) conducted by hand milling (filled symbols) and ball milling (open symbols).

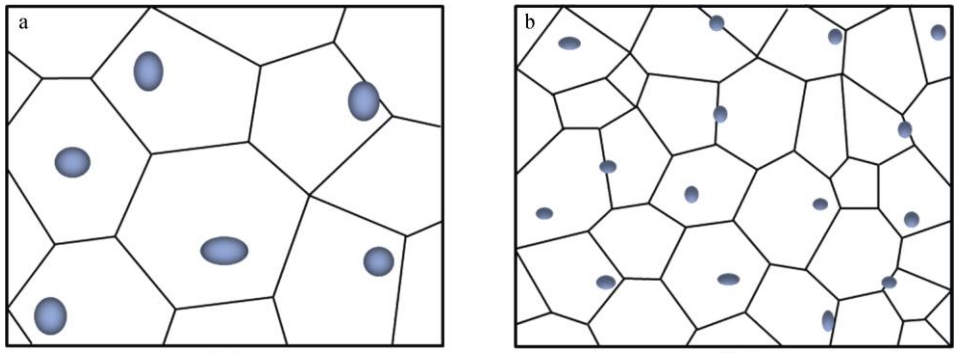

Fig.6 Schematic of SnSe/Ag_2Se composites conducted by **a** hand milling and **b** ball milling.

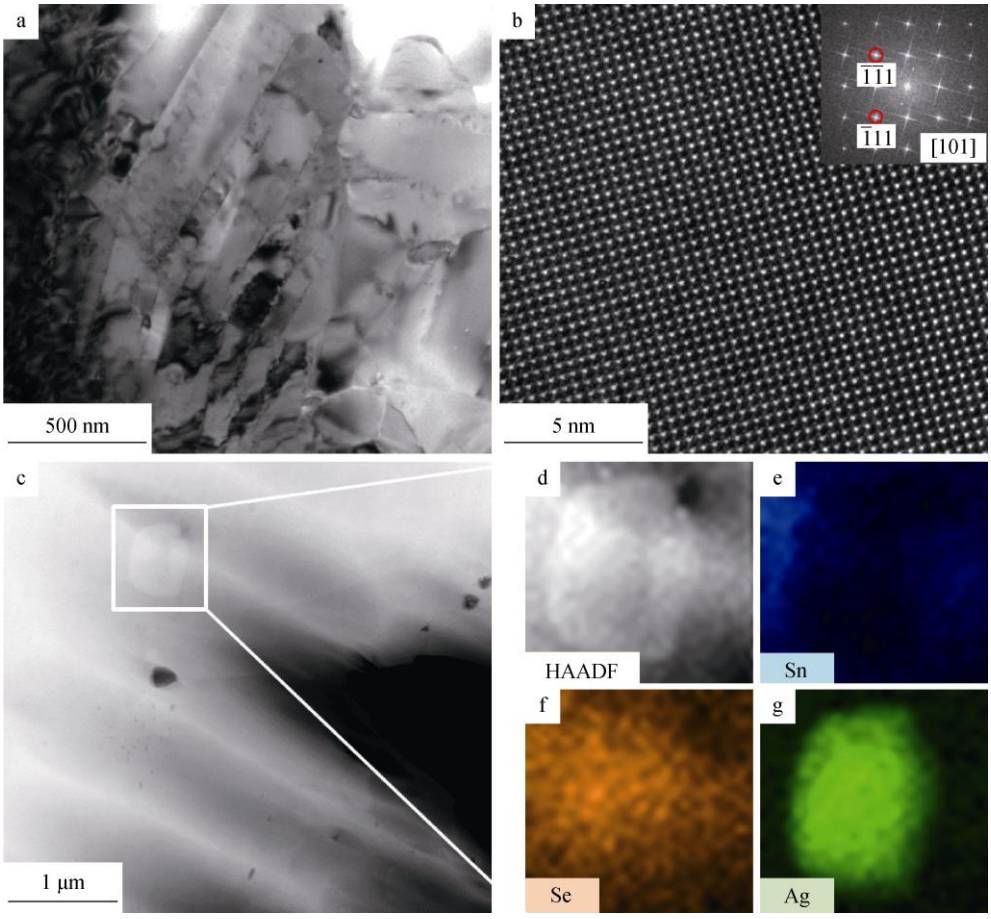

Fig.7 Microstructure of SnSe+1%Ag_2Se conducted by ball milling: **a** low-magnification TEM image, **b** high-resolution transmission electron microscopy (HRTEM) image with FFT pattern (inset), **c** low-magnification HAADF-STEM image, **d** enlarged HAADF-STEM image, and **e-g** corresponding spectrum images of Sn/Se/Ag.

Table 1 Carrier concentration and Hall mobility of SnSe + *x* %Ag_2Se (*x* = 0, 0.5, 1.0 and 3.0) conducted by hand milling and measured parallel and vertical to press direction.

Material	Carrier concentration/($10^{19}cm^{-3}$)		Hall mobility/($cm^2 \cdot V^{-1} \cdot s^{-1}$)	
	Parallel direction	Vertical direction	Parallel direction	Vertical direction
SnSe	0.0468	0.0408	0.158	0.479
SnSe + 0.5%Ag_2Se	0.8870	0.9000	0.147	0.468
SnSe + 1% Ag_2Se	0.8150	0.8190	0.168	0.386
SnSe + 3% Ag_2Se	0.8780	0.8740	0.124	0.255

Supporting information：

SnSe + Ag_2Se composite engineering with ball milling for enhanced thermoelectric performance

Dan Feng[1,2], Yue-Xing Chen[2, 4], Liang-Wei Fu[2], Ju Li[1,3], Jia-Qing He[2,*]

[1]State Key Laboratory for Mechanical Behavior of Materials and Frontier Institute of Science and Technology, Xi'an Jiaotong University, Xi'an 710049, China.
[2]Shenzhen Key Laboratory of Thermoelectric Materials, Department of physics, South University of Science and Technology of China, Shenzhen 518055, China.
[3]Department of Nuclear Science and Engineering and Department of Materials Science and Engineering, Massachusetts Institute of Technology, Cambridge, Massachusetts 02139, USA
[4]Key Laboratory of Artificial Micro- and Nano-Structures of Ministry of Education, School of Physics and Technology, Wuhan University, Wuhan 430072, China

Email: liju@mit.edu, he.jq@sustc.edu.cn

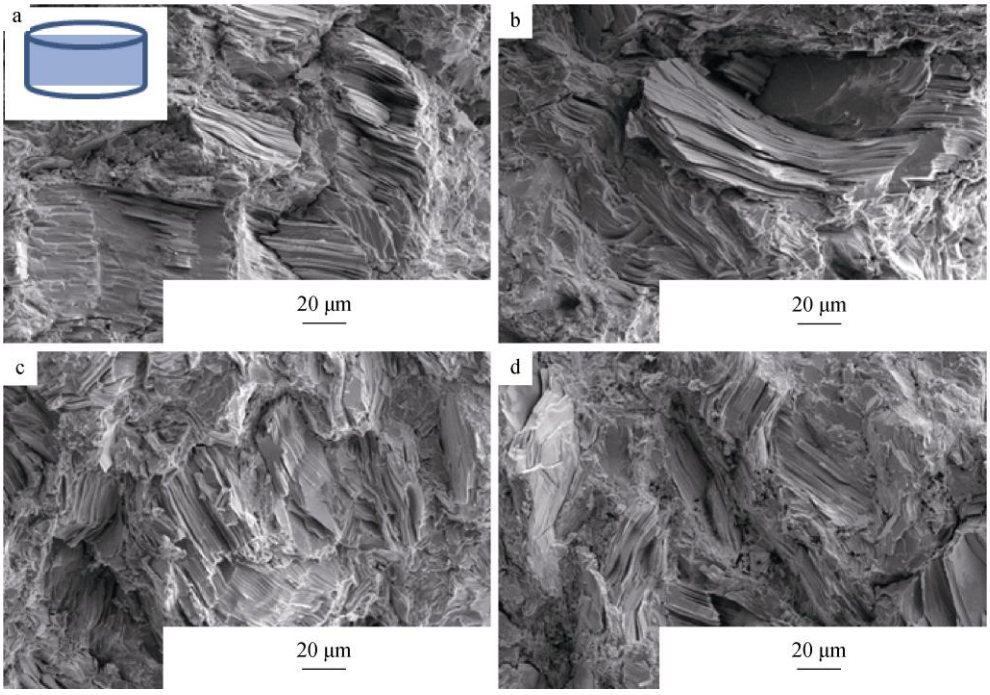

Fig.S1 SEM images of SnSe + *x* %Ag_2Se (*x* = 0, 0.5, 1.0 and 3.0) conducted by hand milling viewed along direction vertical to pressing direction: **a** SnSe-HM, **b** SnSe + 0.5 %Ag_2Se-HM, **c** SnSe + 1.0 %Ag_2Se-HM, and **d** SnSe + 3.0 %Ag_2Se-HM

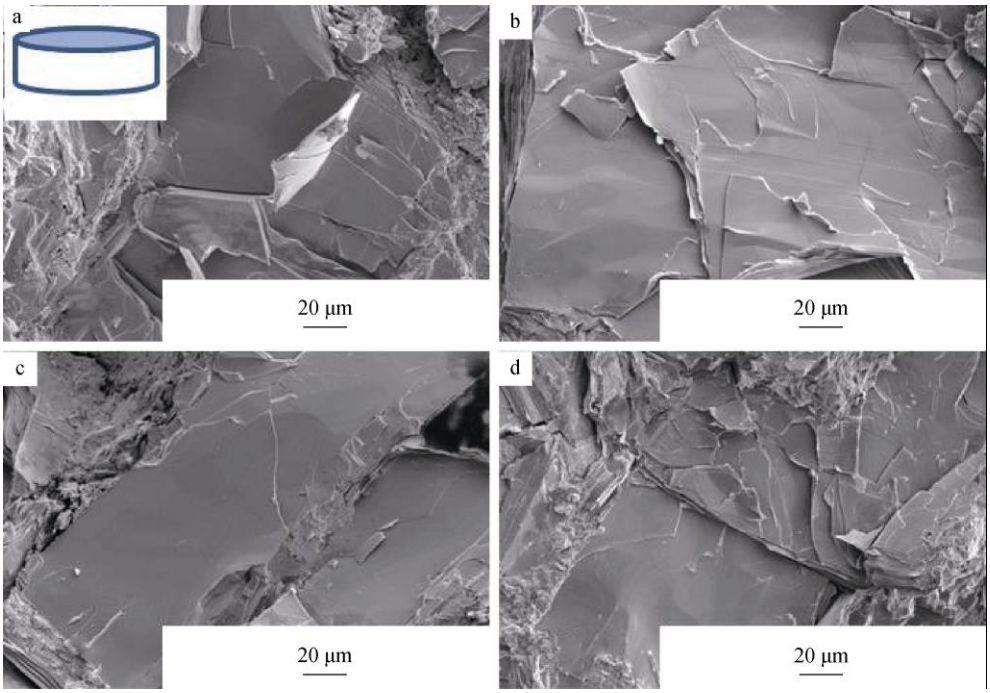

Fig.S2 SEM images of SnSe + *x* %Ag_2Se (*x* = 0, 0.5, 1.0 and 3.0) conducted by hand milling viewed along direction parallel to pressing direction: **a** SnSe-HM, **b** SnSe + 0.5 %Ag_2Se-HM, **c** SnSe + 1.0 %Ag_2Se-HM, and **d** SnSe + 3.0 %Ag_2Se-HM

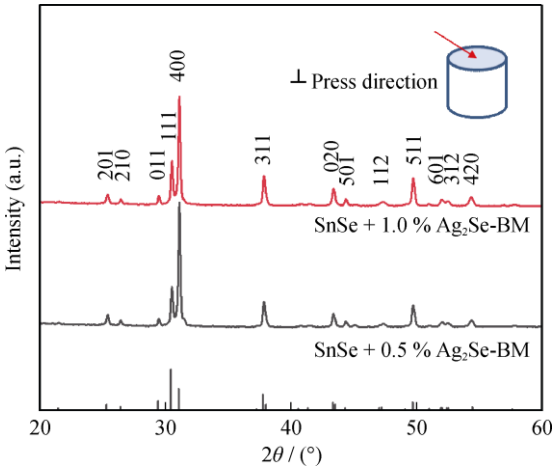

Fig.S3 XRD patterns of SnSe + *x* %Ag_2Se (*x*=0.5, 1.0) conducted by ball milling along direction vertical to pressing direction